Wavefunction embedding for molecular polaritons

Cite as: J. Chem. Phys. (in press) (2022); https://doi.org/10.1063/5.0095552
Submitted: 11 April 2022 • Accepted: 27 June 2022 • Accepted Manuscript Online: 05 July 2022

Fabijan Pavosevic and Angel Rubio

Accepted to J. Chem. Phys. 10.1063/5.0095552

Wavefunction embedding for molecular polaritons

Fabijan Pavošević[1] and Angel Rubio[1, 2, 3]
[1)]*Center for Computational Quantum Physics, Flatiron Institute, 162 5th Ave., New York, 10010 NY, USA*
[2)]*Max Planck Institute for the Structure and Dynamics of Matter and Center for Free-Electron Laser Science & Department of Physics, Luruper Chaussee 149, 22761 Hamburg, Germany*
[3)]*Nano-Bio Spectroscopy Group and European Theoretical Spectroscopy Facility (ETSF), Universidad del País Vasco (UPV/EHU), Av. Tolosa 72, 20018 San Sebastian, Spain*

(*Electronic mail: angel.rubio@mpsd.mpg.de)

(*Electronic mail: fpavosevic@gmail.com)

Polaritonic chemistry relies on the strong light-matter interaction phenomena for altering the chemical reaction rates inside optical cavities. To explain and to understand these processes, the development of reliable theoretical models is essential. While computationally efficient quantum electrodynamics self-consistent field (QED-SCF) methods, such as quantum electrodynamics density functional theory (QEDFT) needs accurate functionals, quantum electrodynamics coupled cluster (QED-CC) methods provide a systematic increase in accuracy but at much greater cost. To overcome this computational bottleneck, herein we introduce and develop the QED-CC-in-QED-SCF projection-based embedding method that inherits all the favorable properties from the two worlds, computational efficiency and accuracy. The performance of the embedding method is assessed by studying some prototypical but relevant reactions, such as methyl transfer reaction, proton transfer reaction, as well as protonation reaction in a complex environment. The results obtained with the new embedding method are in excellent agreement with more expensive QED-CC results. The analysis performed on these reactions indicate that the electron-photon correlation effects are local in nature and that only a small region should be treated at the QED-CC level for capturing important effects due to cavity. This work sets the stage for future developments of polaritonic quantum chemistry methods and it will serve as a guideline for development of other polaritonic embedding models.

I. INTRODUCTION

The ability to control the rates of chemical reactions is the "Holy Grail" sought by chemists, and the strong light-matter interactions created by quantum fluctuations or external pumping in optical or nanoplasmonic cavities offer a non-intrusive way to modulate the rates of chemical reactions. In a newly emerging field of polaritonic chemistry, such strong light-matter coupling effects are utilized to catalyze,[1–3] inhibit,[4,5] or modify the overall reaction path[6,7] of a given chemical reaction. Naturally, these experimental advances have been accompanied by various theoretical developments[2,6,8–14] that attempt to provide an insight into fundamental understanding of the strong light-matter interaction as well as for guiding design principles of processes inside cavities.[8]

Like in the case of the conventional electronic structure methods, there are two main approaches to solve the Schrödinger equation that accounts for the strong light-matter interaction. One is with the density functional theory, and another is based on the wave function theory. In the quantum electrodynamics density functional theory (QEDFT) approach[15–18] both photons and electrons are treated quantum mechanically on the equal footing via a generalized matter-photon exchange-correlation functional. This method is favored for its ability to balance the accuracy and the computational cost, making it suitable for treatment of large molecular systems, and it effectively captures most important effects arising from the strong light-matter coupling.[19] However, the practical implementation of the QEDFT method so far has similar issues that are inherent to the conventional electronic DFT method, such as problems associated with self-interaction error[20] and dispersion interactions.[21] Despite promising directions in designing exchange-correlation functionals, only relatively small number of the exchange-correlation functionals[22,23] for polaritonic problems are currently available. An alternative to QEDFT, but in principle more costly, are systematically improvable wave function based methods such as quantum electrodynamics coupled cluster (QED-CC) method.[24,25] Although the practical implementations of this method rely on numerous approximations and assumptions with plenty of room for further developments,[25] the QED-CC method retains many favorable properties of the electronic CC method such as the size-extensivity,[26] and high accuracy as demonstrated for different chemical processes in optical cavities.[27–31] However, due to a steep polynomial scaling, its applicability is limited to very small molecular systems.

One way for extending the range of applicability of the QED-CC method can be achieved within the quantum many body embedding approach. In this approach,[32] only a small region or chemically active subsystem is treated at a high level theory, whereas the rest of the system (environment subsystem) is described with a lower level theory. Among various embedding approaches,[32–34] a particularly popular and robust is the projection-based embedding method.[35,36] In this method, the orthogonality of occupied orbitals between the active subsystem and the environment subsystem is achieved via the level shift projection operator, that shifts the occupied orbital energies of the environment subsystem to higher energies.[35] This ensures that the sum of energies of both fragments is equal to the energy of the full system if both fragments are

treated at the same level of theory. Therefore, this method is also referred as exact SCF-in-SCF embedding method,[35] where SCF (Self-Consistent Field) can either be the Hartree-Fock (HF) or DFT method. Yet another appealing feature of the projection based embedding is that the correlation energy of the active subsystem is obtained seamlessly without any modification of the post-SCF code. The computational savings comes from the fact that the correlation energy is calculated with a fewer occupied orbitals. For instance, the coupled cluster with singles and doubles (CCSD) scales as $\mathcal{O}(o^2v^4)$, where o and v are the number of occupied and virtual (unoccupied) orbitals, respectively. Within the projection-based embedding method the scaling for solving the CCSD equations is reduced to $\mathcal{O}(v^4)$,[36] whereas non-iterative orbital transformation scales as $\mathcal{O}(N^4v)$, where N is number of basis functions. Additional computational savings are achieved by selecting the unoccupied (virtual) orbitals that are relevant for the embedded subsystem.[37–39] In principle, such truncation of the virtual subspace ensures that the computational cost of the embedding region is independent of the system size.[37,39]

Encouraged by an impressive performance of the projection-based embedding as already implemented in widely used Molpro quantum chemistry software,[40] as well as by robustness of the QED-CC method, in this work we develop the exact QED-SCF-in-QED-SCF projection-based embedding method as well as the QED-CC-in-QED-SCF method for polaritonic systems. In analogy to electronic structure methods, QED-SCF can either be the QED-HF or QED-DFT method. Note that unlike the QEDFT method that was discussed earlier in the introduction, the QED-DFT method employed in this work only includes the correlation effects between electrons through the exchange-correlation functional and it does not include the electron-photon correlation effects. The accuracy and computational performance of the newly developed QED-CC-in-QED-SCF method is verified and benchmarked on the Menshutkin reaction, intramolecular proton transfer reaction in the Z-3-aminopropenal (aminopropenal) molecule, and on the proton binding energy of methanol in the explicit water solvent. The developments and analysis presented in this work highlight the capabilities, versatility, and numerical efficiency of the QED-CC-in-SCF method for accurate description of strong-light matter interaction effect created in optical and nanoplasmonic cavities. It also showcases that only a small part of the system should be treated at a high level of theory for achieving an accurate description of the effects due to cavity. Moreover, this work lays the foundation for developments of other theoretical models in polaritonic chemistry, that will lead to further fundamental understanding of the role of the complex environment in an optical cavity, and it will serve as a guideline and a benchmark for development of other embedding models. To the best of our knowledge, this is the first multi-scale embedding method for treatment of molecular polaritons and it has a tremendous potential for applications to large molecular polaritonic ensembles.

II. THEORY

The quantum mechanical non-relativistic treatment of interaction between molecules and photons inside an optical cavity can be described by the Pauli-Fierz Hamiltonian.[8,15] This Hamiltonian (in atomic units unless otherwise stated), within the dipole approximation (we assume the wavelength of the cavity is much larger than the molecule), in the length gauge,[18,41] in the coherent state basis,[8,25] and for a single cavity photon mode (extension to many cavity modes is, in principle, straightforward) reads as

$$\begin{aligned}\hat{H} = h_q^p a_p^q + \frac{1}{2} g_{rs}^{pq} a_{pq}^{rs} + \omega_{\text{cav}} b^\dagger b \\ - \sqrt{\frac{\omega_{\text{cav}}}{2}} (\boldsymbol{\lambda} \cdot \Delta \boldsymbol{d})(b^\dagger + b) + \frac{1}{2} (\boldsymbol{\lambda} \cdot \Delta \boldsymbol{d})^2.\end{aligned} \tag{1}$$

The first two terms constitute the electronic Hamiltonian (within the Born-Oppenheimer approximation, although non-adiabatic effects can also be incorporated[42–44]) that is defined in terms of the second-quantized electronic excitation operator $a_{p_1 p_2 \dots p_n}^{q_1 q_2 \dots q_n} = a_{q_1}^\dagger a_{q_2}^\dagger \dots a_{q_n}^\dagger a_{p_n} \dots a_{p_2} a_{p_1}$ where $a^\dagger/a$ are fermionic creation/annihilation operators. Moreover, $h_q^p = \langle q|\hat{h}^{\text{e}}|p\rangle$ and $g_{rs}^{pq} = \langle rs|pq\rangle$ is the core electronic Hamiltonian matrix element and the two-electron repulsion tensor element, respectively. The indices $i,j,k,l,\dots$, $a,b,c,d,\dots$, and $p,q,r,s,\dots$ denote occupied, unoccupied, and general electronic spin orbitals, respectively. The third term denotes the oscillation of the single cavity mode with a fundamental frequency ω_{cav} expressed in terms of bosonic creation/annihilation ($b^\dagger/b$) operators. The fourth term describes the dipolar coupling between electronic and photonic degrees of freedom, where $\boldsymbol{\lambda}$ is the light-matter coupling strength vector, and $\Delta\boldsymbol{d} = \boldsymbol{d} - \langle \boldsymbol{d} \rangle$ is the dipole fluctuation operator that denotes the change of the molecular dipole operator with respect to its expectation value. $\boldsymbol{\lambda}$ defines the strength of the light-matter coupling which in turn depends on the permittivity of the vacuum ε_0 and the effective quantization volume (V_{eff}) as $\lambda = 1/\sqrt{\varepsilon_0 V_{\text{eff}}}$.[3,45] This V_{eff} depends on the specific experimental realizations of the optical cavity, and experiments in picocavity setups with effective volume < 1 nm^3 (which corresponds to values of λ around 0.1 a.u.) have been recently achieved.[46–49] Lastly, the fifth term in Eq. (1) describes the dipole self energy.[18,50,51] It is important to add that the role of this term is a very active topic of discussion in the literature and its necessity for certain experimental setups is debated.[52] The dipole self energy term naturally arises in the momentum to the length gauge Power-Zienau-Woolley (PWZ) transformation[53] for transversal (free-space) electromagnetic fields. In the case where only a finite number of cavity modes is considered (such as in the present work), this term has to be accounted to ensure the origin invariance of the Hamiltonian and its boundness from below (i.e., for avoiding the "ground-state catastrophe").[18,50,54,55] For situations where the molecule strongly couples to materials excitations (longitudinal electromagnetic modes) such as in plasmonic nanocavities, it is recommended that the dipole self energy term should not be included,[45,56] however, to ensure a bounded spectrum

Accepted to J. Chem. Phys. 10.1063/5.0095552

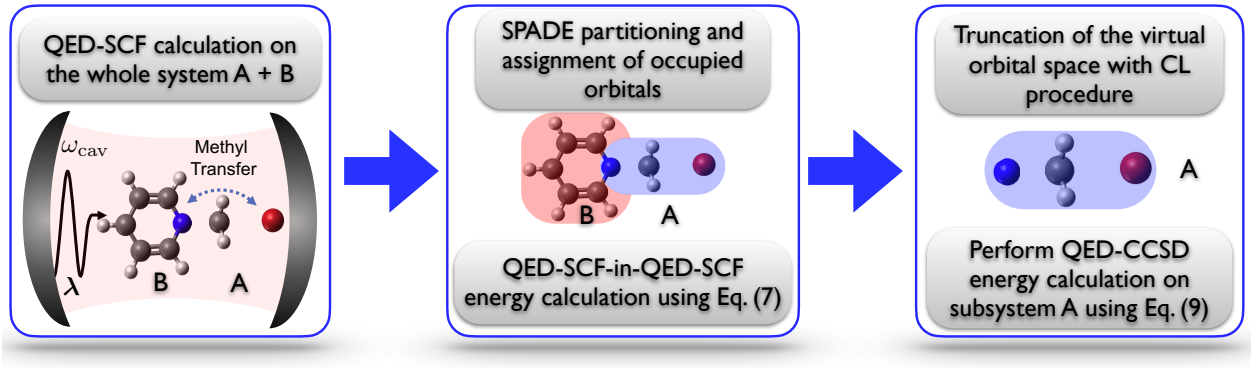

FIG. 1. Schematic depiction of the steps performed in the embedding QED-CCSD-in-QED-SCF method.

and origin invariance of the Hamiltonian beyond dipole corrections have to be included.[57]

Just like in conventional electronic structure methods, the usual starting point for the accurate correlated methods is the quantum electrodynamics Hartree-Fock (QED-HF) method,[25] in which the wave function ansatz

$$|0^{\mathrm{e}}0^{\mathrm{ph}}\rangle = |0^{\mathrm{e}}\rangle \otimes |0^{\mathrm{ph}}\rangle \tag{2}$$

is expressed as a direct product between an electronic Slater determinant $|0^{\mathrm{e}}\rangle$ and a photon-number state $|0^{\mathrm{ph}}\rangle$, where the superscripts e and ph denote electrons and photons, respectively. Because the QED-HF method treats the electrons and photons as uncorrelated particles that interact through the mean-field potential, the predictions obtained from this method are often inaccurate and unreliable.[27,31] Within the QED-HF procedure, the correlation effects between electrons can be simply included by adding the exchange-correlation potential to the working QED-HF equations, which defines the QED-DFT method. Note that unlike the QEDFT method, the QED-DFT method will lack the important electron-photon correlation effects. In QED-CC,[25] the correlation effects between quantum electrons and photons are accounted through the exponentiated form of the cluster operator

$$\hat{T} = \sum_{\mu,n} t_{\mu,n} a^{\mu} (b^{\dagger})^{n} \tag{3}$$

as

$$|\Psi_{\text{QED-CC}}\rangle = e^{\hat{T}} |0^{\mathrm{e}}0^{\mathrm{ph}}\rangle. \tag{4}$$

The unknown wave function parameters $t_{\mu,n}$ (amplitudes) are determined by solving a set of nonlinear equations

$$\langle 0^{\mathrm{e}}0^{\mathrm{ph}}| a_{\mu} (b)^{n} e^{-\hat{T}} \hat{H} e^{\hat{T}} |0^{\mathrm{e}}0^{\mathrm{ph}}\rangle = \sigma_{\mu,n}. \tag{5}$$

Here, $a^{\mu} = a^{\dagger}_{\mu} = \{a^{a}_{i}, a^{ab}_{ij}, \ldots\}$ is the electronic excitation operator, the index μ is the electronic excitation manifold (rank), and n corresponds to the number of photons. Truncation of the cluster operator to include up to single and double electronic excitations along with their interactions with up to two quantum photons is expressed as

$$\begin{aligned}\hat{T} = {} & t^{i,0}_{a} a^{a}_{i} + t^{0,1} b^{\dagger} + \frac{1}{4} t^{ij,0}_{ab} a^{ab}_{ij} + t^{i,1}_{a} a^{a}_{i} b^{\dagger} + \frac{1}{4} t^{ij,1}_{ab} a^{ab}_{ij} b^{\dagger} \\ & + t^{0,2} b^{\dagger} b^{\dagger} + t^{i,2}_{a} a^{a}_{i} b^{\dagger} b^{\dagger} + \frac{1}{4} t^{ij,2}_{ab} a^{ab}_{ij} b^{\dagger} b^{\dagger},\end{aligned} \tag{6}$$

and defines the QED-CCSD-22 method[29,31] that we will simply refer as QED-CCSD in the remainder of this article.

Next, we will briefly describe the QED projection-based quantum embedding technique which works in analogous way to its conventional electronic counterpart. This approach starts by first performing the QED-SCF calculation (QED-HF or QED-DFT) that provides molecular orbitals. These orbitals along with their corresponding density matrices γ are then partition into the active subsystem A and the environment subsystem B. In this work we use the Subsystem Projected Atomic-orbital Decomposition (SPADE)[58] procedure for partitioning of the full system into the subsystems A and B. We note that also other partitioning procedures are possible, such as partitioning via a combination of Pipek-Mezey (PM) orbital localization[59] and Mulliken population screening[60] or partitioning the system density based on von Neumann entropy.[61] After the whole system is partitioned, the energy expression of the subsystem A embedded in subsystem B is

$$\begin{aligned}& E_{\text{QED-SCF-in-QED-SCF}}[\gamma^{\mathrm{A}}_{\mathrm{emb}}; \gamma^{\mathrm{A}}, \gamma^{\mathrm{B}}] = \\ & E_{\text{QED-SCF}}[\gamma^{\mathrm{A}}_{\mathrm{emb}}] + E_{\text{QED-SCF}}[\gamma^{\mathrm{A}} + \gamma^{\mathrm{B}}] - E_{\text{QED-SCF}}[\gamma^{\mathrm{A}}] \\ & + \mathrm{tr}[(\gamma^{\mathrm{A}}_{\mathrm{emb}} - \gamma^{\mathrm{A}}) v_{\mathrm{emb}}[\gamma^{\mathrm{A}}, \gamma^{\mathrm{B}}]] + \alpha \mathrm{tr}[\gamma^{\mathrm{A}}_{\mathrm{emb}} \mathbf{P}].\end{aligned} \tag{7}$$

where $\gamma^{\mathrm{A}}_{\mathrm{emb}}$ is the density matrix of the embedded subsystem A, $E_{\text{QED-SCF}}$ is the QED-HF or QED-DFT energy evaluated with a given density, $\mathbf{P}$ is a projector that ensures orthogonality of orbitals between subsystems, α is the level-shift parameter that shifts orbital energies of subsystem B to infinity (recommended value for α as well as used in this work is 10^6 a.u.[35]), and finally v_{emb} is the embedding potential defined as

$$v_{\mathrm{emb}}[\gamma^{\mathrm{A}}, \gamma^{\mathrm{B}}] = \tilde{g}[\gamma^{\mathrm{A}} + \gamma^{\mathrm{B}}] - \tilde{g}[\gamma^{\mathrm{A}}]. \tag{8}$$

In this equation, $\tilde{g}$ includes all two-electron terms such as the Coulomb, exchange, dipole self energy, as well as the electronic exchange-correlation contributions in case of the QED-DFT method. It is important to note that the projection-based

embedding approach is free from non-additive kinetic energy problem.[35] As a result, if both fragments are treated at the same QED-SCF level, then the QED-SCF-in-QED-SCF embedding calculation is equivalent to performing the QED-SCF calculation on the whole system. The described QED-SCF-in-QED-SCF embedding method given by Eq. (7) sets the stage for the QED-CCSD-in-QED-SCF embedding method, where the active subsystem A is treated using the QED-CCSD method from Eq. (6) and environment subsystem B is described with the QED-SCF method. Then the QED-CCSD-in-QED-SCF energy is simply obtained by substituting the QED-SCF energy of the subsystem A with the QED-CCSD energy as

$$\begin{aligned} &E_{\text{QED-CCSD-in-QED-SCF}}[\Psi^{\text{A}}_{\text{QED-CCSD}};\gamma^{\text{A}},\gamma^{\text{B}}] = \\ &E_{\text{QED-CCSD}}[\Psi^{\text{A}}_{\text{QED-CCSD}}] + E_{\text{QED-SCF}}[\gamma^{\text{A}}+\gamma^{\text{B}}] \\ &- E_{\text{QED-SCF}}[\gamma^{\text{A}}] + \text{tr}[(\gamma^{\text{A}}_{\text{emb}}-\gamma^{\text{A}})\boldsymbol{v}_{\text{emb}}[\gamma^{\text{A}},\gamma^{\text{B}}]] \\ &+ \alpha\text{tr}[\gamma^{\text{A}}_{\text{emb}}\mathbf{P}]. \end{aligned} \tag{9}$$

Here, $\Psi^{\text{A}}_{\text{QED-CCSD}}$ is the wave function of the subsystem A that determines the embedding density matrix $\gamma^{\text{A}}_{\text{emb}}$, and $E_{\text{QED-CCSD}}[\Psi^{\text{A}}_{\text{QED-CCSD}}]$ is the QED-CCSD energy evaluated with $\Psi^{\text{A}}_{\text{QED-CCSD}}$. In the remainder of this article we will refer to QED-CCSD-in-QED-SCF simply as QED-CCSD-in-SCF. Schematic depiction of the workflow for the QED-CC-in-QED-SCF method is given in Fig. 1.

III. RESULTS

The QED-CCSD-in-SCF embedding method have been implemented in an in-house version of the Psi4NumPy quantum chemistry software.[62] The calculations to study the Menshutkin reaction were performed on the geometries optimized at the conventional electronic MP2/6-31G(d)[63–65] level using the Orca quantum chemistry software.[66] The calculations to study the proton transfer in aminopropenal molecule were performed on the geometries optimized at the conventional electronic CCSD/cc-pVDZ level.[67] The geometries of the optimized structures (reactants, transition states, and products) are provided in the supplementary material. The cavity effect on the proton binding energy of methanol in an explicit water solvent was performed on geometries obtained from Ref. 68. All of the QED-SCF calculations are carried out with the HF method, as well as with the PBE,[69] and hybrid PBE0[70] and B3LYP[71,72] functionals. Moreover, all of the QED calculations employ $\omega_{\text{cav}} = 3$ eV and $\lambda = 0.1$ a.u. cavity parameters unless otherwise noted. The calculated molecular volumes of the three systems used in this work are $V_{\text{mol}} = 0.171$ nm^3 for the Menshutkin reaction complex, $V_{\text{mol}} = 0.093$ nm^3 for the aminopropenal molecule, and $V_{\text{mol}} = 0.158$ nm ^{3} for the methanol in five water molecules, which are all smaller than the effective quantization volume ($V_{\text{eff}} = 0.19$ nm^3) that corresponds to $\lambda = 0.1$ a.u. The calculated molecular volume is defined as the volume inside a contour of 0.001 electrons/Bohr^3 ground state electron density, where the density is obtained with the B3LYP/cc-pVDZ method. The partitioning of the full system into the subsystems A and B is performed with the Subsystem Projected Atomic-orbital Decomposition (SPADE)[58] procedure. Truncation of the virtual (unoccupied) orbital space is carried out by employing the Concentric Localization (CL) of orbitals[39] procedure, which can be viewed as an extension of the SPADE procedure for partitioning of the unoccupied orbitals. All of the CL calculations employ two CL shells unless otherwise noted. Moreover, the projection basis set used in the CL calculations is the same as the working basis set (i.e. 6-31G(d) for the Menshutkin reaction, and cc-pVDZ for the proton transfer reaction and the proton binding energy of methanol).

In our first example, we study the effect of optical cavity on the Menshutkin S_N2 reaction. Figure 2 shows the reaction energy diagram of the nucleophilic methyl transfer process in pyridine with methyl bromide calculated with the PBE0, CCSD, and CCSD-in-PBE0 methods (solid lines) along with their QED counterparts (dashed lines) employing the 6-31G(d) basis set.[63–65] The QED calculations were performed with cavity mode polarized along the x (left panel) and z (right panel) directions and by employing $\omega_{\text{cav}} = 3$ eV and $\lambda = 0.1$ a.u. cavity parameters that are both within the range of current experimental setups[73,74] as discussed earlier in the text. Moreover, Fig. 2 indicates partitioning of the full system into the subsystem A (blue domain) and the subsystem B (red domain). The subsystem A is treated with the QED-CCSD method and the subsystem B is treated with the QED-SCF method. The effects of the cavity on change in the reaction energies and barriers for the cavity polarized along the x, y, and z directions calculated with the QED-HF, QED-PBE, QED-PBE0, QED-B3LYP, QED-CCSD, QED-CCSD-in-HF, QED-CCSD-in-PBE, QED-CCSD-in-PBE0, and QED-CCSD-in-B3LYP methods using the 6-31G(d) basis set[63–65] are provided in Table I. This Table shows that all the embedding methods are in excellent agreement with the QED-CCSD method, and that they are able to accurately describe changes in the energy reactions and barriers due to cavity.

As shown in Fig. 2, the reaction barrier for the methyl transfer depends on the choice of the electronic structure method, where PBE0 underestimates the reaction barrier by $\sim$3 kcal/mol relative to the CCSD method. The embedding CCSD-in-PBE0 method shows better agreement relative to CCSD, where the reaction barrier is overestimated by only $\sim$1 kcal/mol. We note that extension of the embedding domain to include two adjacent CH groups will reduce this discrepancy to $\sim$0.2 kcal/mol. More information about performance of different SCF and CCSD-in-SCF methods, as well as different embedding domains is provided in Table S1 of the supplementary material. The QED-HF, QED-PBE, QED-PBE0, and QED-B3LYP methods predicts increase in reaction barrier when the cavity mode is polarized along the x direction, which is in stark contrast relative to the QED-CCSD method that predicts decrease in reaction barrier. This discrepancy is due to lack of the electron-photon correlation effects in the QED-SCF methods. All of the embedding QED-CCSD-in-HF, QED-CCSD-in-PBE, QED-CCSD-in-PBE0, and QED-CCSD-in-B3LYP methods predicts the same qualitative trend as the QED-CCSD method. This important finding indicates

Accepted to J. Chem. Phys. 10.1063/5.0095552

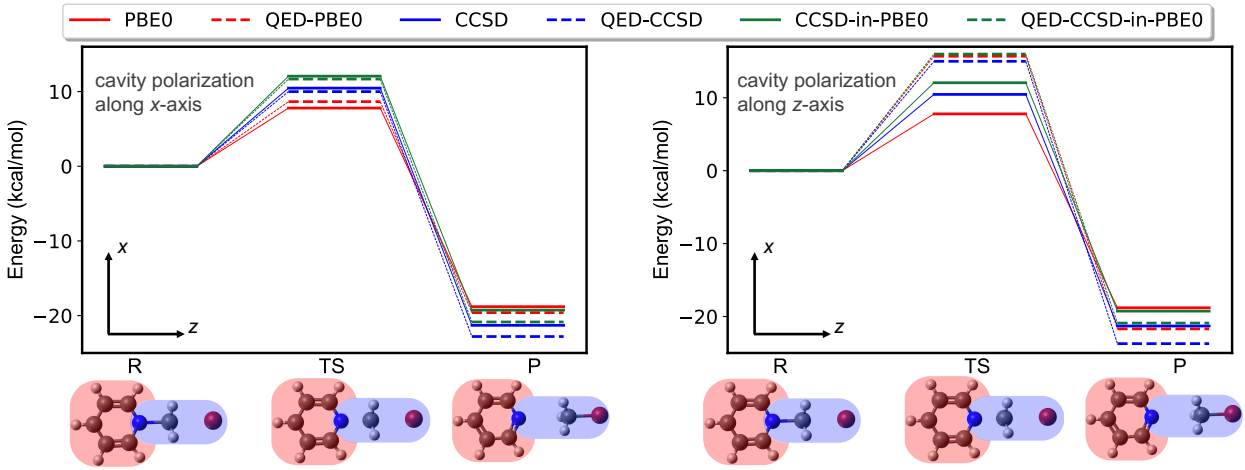

FIG. 2. Reaction diagram for methyl transfer in pyridine with methyl bromide calculated with PBE0 (red), CCSD (blue), and CCSD-in-PBE0 (green) outside (solid) and inside (dashed) an optical cavity utilizing the 6-31G(d) basis set. The QED calculations employ $\omega_{\text{cav}} = 3$ eV and $\lambda = 0.1$ a.u. cavity parameters with the photon mode polarized along the x (left panel), and z (right panel) directions. The images of reactant (R), transition state (TS), and product (P) structures also depict the subsystem A in blue (treated with CCSD/QED-CCSD) and subsystem B in red (treated with PBE0/QED-PBE0).

TABLE I. Change in the reaction energy barrier (TS)[a] and reaction energy (ΔE)[b] (in kcal/mol) for methyl transfer in pyridine with methyl bromide inside an optical cavity.

method	x direction		y direction		z direction	
	TS	ΔE	TS	ΔE	TS	ΔE
QED-HF	0.39	-0.84	-0.22	-1.88	5.00	1.01
QED-PBE	1.63	0.38	-0.18	-1.75	5.38	-7.85
QED-PBE0	0.86	-0.51	-0.38	-2.01	8.07	-2.38
QED-B3LYP	1.06	-0.30	-0.35	-1.94	7.50	-3.10
QED-CCSD	-0.50	-1.55	-0.38	-1.38	3.45	-2.41
QED-CCSD-in-HF	-0.22	-1.34	-0.42	-1.70	3.69	-2.09
QED-CCSD-in-PBE	-0.65	-1.89	-0.45	-1.72	4.67	-1.19
QED-CCSD-in-PBE0	-0.42	-1.63	-0.41	-1.66	4.05	-1.88
QED-CCSD-in-B3LYP	-0.47	-1.66	-0.43	-1.70	4.09	-1.73

[a]Effect of the cavity on the reaction energy barrier is calculated as the difference between the reaction energy barrier obtained with the QED method and the corresponding conventional electronic structure method.

[b]Effect of the cavity on the on the reaction energy (i.e., the difference between the energies of the product and reactant) is calculated as the difference between the reaction energy obtained with the QED method and the corresponding conventional electronic structure method.

the local nature of the electron-photon correlation and that relatively small region can be treated at the high level for qualitatively and quantitatively correct description of the cavity effect. For the cavity mode with polarization along the y direction, all the QED methods predicts a decrease in reaction barrier and they are all in agreement with each other. Lastly, in the case of the cavity mode polarized in the z direction, all studied QED methods predicts an increase of reaction barrier. The greatest increase in the reaction barrier is observed with the QED-SCF methods. Inclusion of the correlation effects between electrons and photons with either the QED-CCSD method or the embedding methods reduces this value by a few kcal/mol.

Next, we discuss the cavity effect on the reaction energy for the same Menshutkin reaction, which is calculated as the energy difference between the product and the reactant. In the case of cavity mode with polarization along the x direction, all of the QED-SCF (i.e. QED-HF, QED-PBE, QED-PBE0, and QED-B3LYP) methods underestimate the effect of the cavity on reaction energy relative to the QED-CCSD method, whereas the embedding methods are in an excellent agreement with the full QED-CCSD method. For the cavity mode with polarization along the y direction, all the QED methods are in agreement with each other. Finally, in the case of cavity with the cavity mode polarized in the z direction, all studied QED methods predict a decrease of the reaction energy in the presence of the optical cavity, whereas the QED-HF method predicts the opposite trend.

Due to relatively small system size, the virtual orbital space is not truncated when using two CL shells. In order to investigate the effect of truncation of the virtual orbital space on the reaction energy profile, we have performed the QED-CCSD-in-PBE0 calculations with one CL shell and the results are given in Table S1 of the supplementary material. With one CL shell, the virtual orbital space is truncated by 37% (71 active virtual orbitals vs. 113 virtual orbitals in total). Although the calculated reaction barrier is overestimated by ~ 2 kcal/mol relative to the CCSD method, the trend due to the cavity polarized in all three directions is maintained compared to calculations with two CL shells.

The upper panel of Fig. 3 shows the effect of cavity on reaction barrier for the Menshutkin reaction as the cavity frequency increases from 0 eV to 10 eV, whereas the lower panel shows the effect of cavity of the same reaction as the cavity coupling strength increases from 0 a.u. to 0.2 a.u. We would like to emphasize that for this value of the light-matter

Accepted to J. Chem. Phys. 10.1063/5.0095552

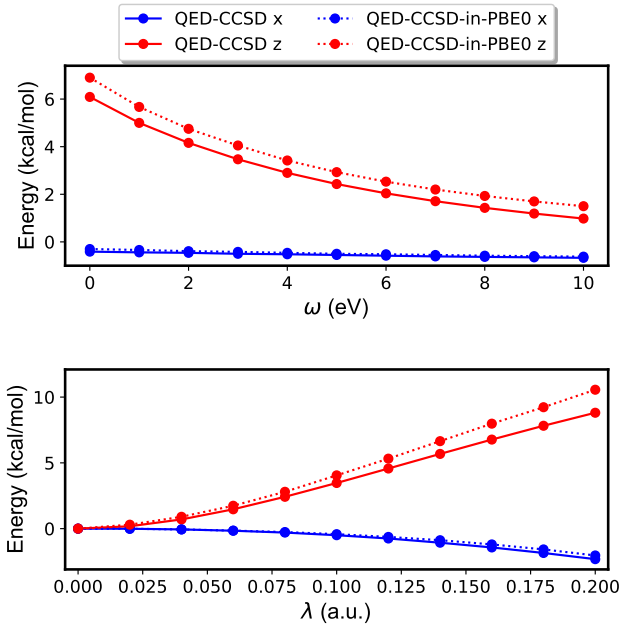

FIG. 3. Change of the reaction barrier for the Menshutkin reaction as a function of cavity frequency (upper panel) and cavity coupling strength (lower panel) inside of optical cavity with light polarized along the x (blue) and z (red) directions. Solid lines correspond to the QED-CCSD calculations, whereas dotted lines correspond to the QED-CCSD-in-PBE0 calculations. The upper panel is calculated with the coupling strength of 0.1 a.u., whereas the lower panel is calculated with the cavity frequency of 3 eV.

coupling ($\lambda = 0.2$ a.u.) the effective quantization volume is only $V_{\text{eff}} = 0.05\text{nm}^3$ which is much smaller that the estimate molecular volume of $V_{\text{mol}} = 0.171\text{nm}^3$ making it experimentally unfeasible. However, in our case such a large value of the coupling strength is used to showcase the robustness and stability of the embedding method for wide range of cavity coupling strength values. The upper and lower panels are calculated for the cavity coupling strength of 0.1 a.u. and for the cavity frequency of 3 eV, respectively. The changes in barriers are calculated with the QED-CCSD method (solid lines) and QED-CCSD-in-PBE0 method (dotted lines) in a cavity with the mode polarized along x (blue lines) and z (red lines) directions. As indicated in Fig. 3, the embedding QED-CCSD-in-PBE0 method is in an excellent agreement with the QED-CCSD method for this ranges of cavity coupling strengths and cavity frequencies. The upper panel also shows that in the case of the cavity mode polarized along the x and z directions the reaction barriers are decreasing as the cavity frequency increases. We note that the QED-SCF methods do not have dependence on cavity frequency as discussed in Ref. 25 and 28. The lower panel shows that in the case of very large values of coupling strength, the reaction barrier decreases by $\sim$2 kcal/mol when cavity mode is polarized along the x direction, whereas when cavity mode is polarized along the z direction the reaction barrier barrier increases by $\sim$10 kcal/mol.

As our next example, we study the effect of optical cavity on the proton transfer in the aminopropenal molecule. Figure 4 shows the reaction energy diagram for proton transfer reaction in the aminopropenal molecule calculated with the PBE0, CCSD, and CCSD-in-PBE0 methods outside cavity (solid lines) and inside cavity (dashed lines) employing the cc-pVDZ basis set.[67] The QED calculations are performed with cavity parameters $\omega_{\text{cav}} = 3$ eV and coupling strength $\lambda = 0.1$ a.u. with light polarized along the x (left) and z (right) directions. Both left and right panels include geometries of reactant (R), transition state (TS), and product (P) along with partitioning of the full system into the subsystem A (blue region) and the subsystem B (red region). Table II provides the changes in reaction energies and barriers calculated with QED-HF, QED-PBE, QED-PBE0, QED-B3LYP, QED-CCSD, QED-CCSD-in-HF, QED-CCSD-in-PBE, QED-CCSD-in-PBE0, and QE-CCSD-in-B3LYP methods with the cavity mode polarized along all three directions. As it was the case for Menshutkin reaction, the reaction energy profile greatly depends on the choice of electronic structure method as indicated in Fig. 4 and Table S2 of the supplementary material. Interestingly, both PBE and PBE0 predict the barrier-less proton transfer reaction using these geometries, whereas the HF, B3LYP, CCSD, and all of the CCSD-in-SCF methods predict the process with the barrier. The HF method greatly overestimates the reaction barrier relative to the CCSD method, whereas the CCSD-in-PBE0 method predicts the barrier that is $\sim$1.5 kcal/mol of the CCSD barrier. Furthermore, all of the CCSD-in-SCF methods predict the reaction energy that is in a good agreement with the CCSD predictions.

TABLE II. Change in the reaction energy barrier (TS)[a] and reaction energy (ΔE)[b] (in kcal/mol) for proton transfer in aminopropenal inside an optical cavity.

method	x direction		y direction		z direction	
	TS	ΔE	TS	ΔE	TS	ΔE
QED-HF	2.00	0.94	0.59	0.37	-0.01	0.06
QED-PBE	2.21	0.81	0.15	-0.18	-0.10	0.00
QED-PBE0	2.27	0.83	0.36	-0.03	-0.07	0.01
QED-B3LYP	2.26	0.82	0.32	-0.07	-0.07	0.01
QED-CCSD	1.07	0.13	0.06	-0.22	-0.33	-0.20
QED-CCSD-in-HF	1.32	0.20	0.00	-0.32	-0.27	-0.23
QED-CCSD-in-PBE	1.72	-0.31	-0.02	-0.30	-0.29	-0.20
QED-CCSD-in-PBE0	1.55	-0.15	-0.03	-0.32	-0.28	-0.21
QED-CCSD-in-B3LYP	1.64	-0.21	-0.03	-0.34	-0.28	-0.22

[a]Effect of the cavity on the reaction energy barrier is calculated as the difference between the reaction energy barrier obtained with the QED method and the corresponding conventional electronic structure method.

[b]Effect of the cavity on the on the reaction energy (i.e., the difference between the energies of the product and reactant) is calculated as the difference between the reaction energy obtained with the QED method and the corresponding conventional electronic structure method.

For the cavity with the mode polarized along the x direction, the greatest increase in the barrier due to cavity is observed for the QED-SCF methods. Inclusion of the electron-photon correlation effects with the QED-CCSD method reduces this change by $\sim$1 kcal/mol. All the embedding QED-CCSD-in-SCF methods show an increase of the barrier that is in be-

Accepted to J. Chem. Phys. 10.1063/5.0095552

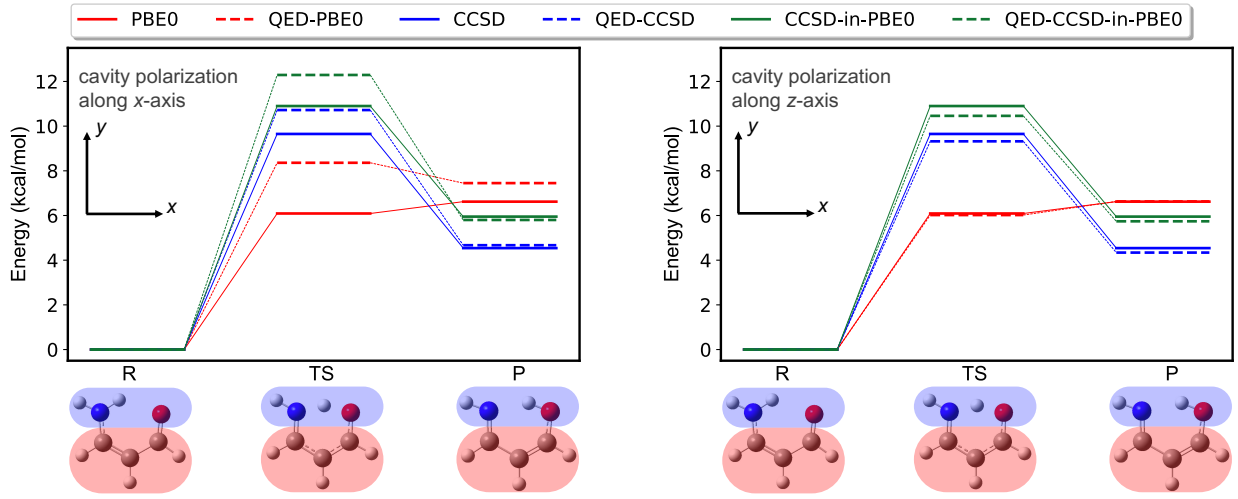

FIG. 4. Reaction diagram for proton transfer in the aminopropenal molecule calculated with PBE0 (red), CCSD (blue), and CCSD-in-PBE0 (green) outside (solid) and inside (dashed) an optical cavity utilizing the cc-pVDZ basis set. The QED calculations employ $\omega_{cav} = 3$ eV and $\lambda = 0.1$ a.u. cavity parameters with the photon mode polarized along the x (left panel), and z (right panel) directions. The images of reactant (R), transition state (TS), and product (P) structures also depict the subsystem A in blue (treated with CCSD/QED-CCSD) and the subsystem B in red (treated with PBE0/QED-PBE0).

tween the one observed with the QED-CCSD and QED-SCF methods. For the cavity mode polarized along the y direction, the QED-CCSD and QED-CCSD-in-SCF methods show very small change (< 0.1 kcal/mol) in barrier due to cavity, whereas the QED-SCF methods predicts more pronounced increase in the reaction barrier. When the cavity mode is polarized along the z direction, all of the QED-SCF methods show a negligible decrease of the reaction barrier, whereas upon inclusion of the correlation effects between electrons and photons with the QED-CCSD and QED-CCSD-in-SCF methods, this change becomes more pronounced. Importantly, all the QED-embedding methods are in an excellent agreement with the QED-CCSD method.

Next, we discuss the effect of the cavity on the reaction energies for the same proton transfer reaction. In the case when the cavity mode is polarized along the x direction, the QED-SCF methods predict significant increase of the reaction energy due to cavity, whereas the QED-CCSD method predicts a more modest change. While QED-CCSD-in-HF is in a good agreement with the QED-CCSD method, the QED-CCSD-in-PBE, QED-CCSD-in-PBE0, and QED-CCSD-in-B3LYP on the other hand predict completely opposite trend. This behaviour may be due to the density-driven error.[75–77] In analogy to conventional electronic structure, this error can be corrected by evaluating the QED-DFT energy in a non-iterative fashion by using more accurate QED-HF density and the resulting method is coined as QED-CCSD-(HF-DFT).[77] The QED-CCSD-in-(HF-PBE0) method predicts increase of reaction barrier by 0.52 kcal/mol which is in a qualitatively good agreement with the QED-CCSD and QED-CCSD-in-HF methods. We also note that other investigated functionals (PBE and B3LYP) predict the same trend, however further investigation is warranted and it is an interesting future research direction. For the cavity with the mode polarized along the y direction, all of the QED-SCF methods, except for the QED-HF method, predict small decrease in reaction energies, whereas for the QED-CCSD and QED-CCSD-in-SCF methods this decrease is slightly more pronounced. Finally, for the cavity mode polarized along the z direction, all of the QED-SCF methods show small increase in the reaction energy due to cavity, whereas the QED-CCSD and QED-CCSD-in-SCF methods predict the opposite trend.

TABLE III. Proton binding energies (in kcal/mol) for methanol in the gas phase and in explicit solvent calculated outside an optical cavity (without optical cavity) and cavity effect on the proton binding energy with and without explicit solvent.

method	MeOH		MeOH-in-5H_2O	
	outside cavity	cavity effect[a]	outside cavity	cavity effect[a]
QED-HF	419.50	0.52	421.43	0.95
QED-PBE	412.70	1.11	407.63	2.54
QED-PBE0	415.64	0.86	413.85	1.63
QED-B3LYP	415.15	0.87	412.30	1.82
QED-CCSD	421.28	1.54	421.38	1.71
QED-CCSD-in-HF	-	-	421.34	1.83
QED-CCSD-in-PBE	-	-	419.53	1.74
QED-CCSD-in-PBE0	-	-	419.65	1.82
QED-CCSD-in-B3LYP	-	-	419.83	1.77

[a] Effect of the cavity on the PBEn is calculated as the difference between the PBEn obtained with the QED method and the corresponding conventional electronic structure method.

As it was the case for the Menshutkin reaction, the virtual orbital space is not truncated when using two CL shells. The results obtained with the QED-CCSD-in-PBE0 method with one CL shell are given in Table S2 of the supplementary material. With one CL shell the virtual orbital space is truncated by 50% (38 active orbitals vs. 76 virtual orbitals is total). As

Accepted to J. Chem. Phys. 10.1063/5.0095552

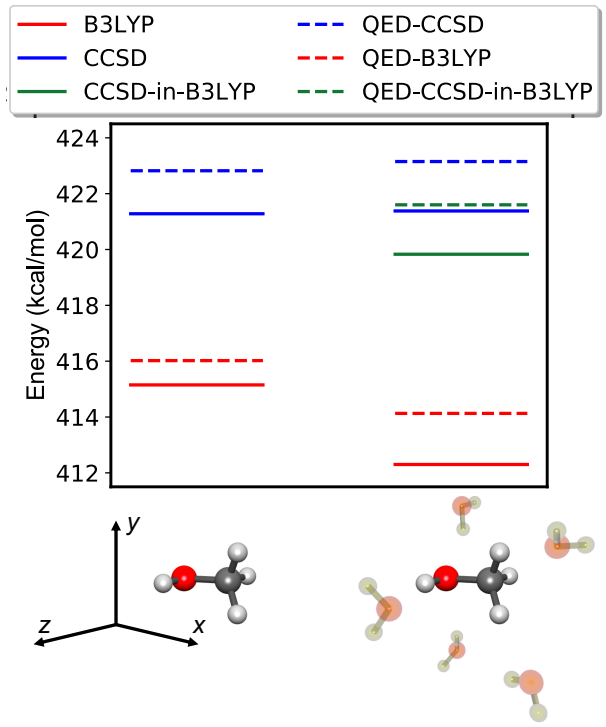

FIG. 5. Proton binding energies (PBEn) for methanol in the gas phase (left) and explicit solvent (right) calculated with the B3LYP, CCSD, and CCSD-in-B3LYP methods outside (solid lines) and inside (dashed lines) optical cavity employing the cc-pVDZ basis set. The QED calculations employ $\omega_{\text{cav}} = 3$ eV and $\lambda = 0.1$ a.u. cavity parameters with the photon mode polarized along the z direction (along dissociating O-H bond). The image of methanol in explicit water are also shown (right).

indicated from the Table S2, all of the results obtained with one CL shell are in qualitatively good agreement with results obtained with two CL shells.

In our last example, we investigate the cavity effect on the proton binding energy (PBEn) for methanol (MeOH) with explicit water solvent. The PBEn is calculated as the energy difference between MeO^- and MeOH. Figure 5 depicts the PBEn for MeOH molecule in the gas phase (left side of Fig. 5) and in explicit solvent consisting of five water molecules (right side of Fig. 5) calculated with the B3LYP, CCSD, and QED-CCSD-in-B3LYP methods outside (solid lines) and inside (dashed lines) the cavity employing the cc-pVDZ basis set.[67] The embedding calculation employs two CL shells where the virtual orbital space is truncated by 28% (96 active virtual orbitals vs. 134 virtual orbitals in total). The QED calculations were performed with the cavity mode polarized along the z direction (along dissociating O-H bond) with the cavity parameters $\omega_{\text{cav}} = 3$ eV and $\lambda = 0.1$ a.u. Moreover, Fig. 5 also contains the coordinate frame along with the MeOH molecule in the gas phase (left) and in an explicit solvent (right). Numerical values of the PBEn calculated with CCSD, different SCF, and CCSD-in-SCF methods outside cavity are given in Table III (columns 1 and 3), and the cavity effect (with light polarized along the z direction) on the PBEn is contained in columns 2 and 4 of the same Table. The effect of the cavity on the PBEn is calculated as the difference between the PBEn obtained with the QED method and the corresponding conventional electronic structure method.

It is indicative that for the investigated system in the gas phase all of the studied QED-SCF methods underestimate the effect of cavity relative to the QED-CCSD predictions. Moreover, the QED-SCF methods predict two fold increase of the PBEn due to cavity upon inclusion of the solvent, whereas this change for the QED-CCSD method remains nearly constant (1.54 kcal/mol vs. 1.76 kcal/mol). This is primarily due to an inadequate treatment of the dipole self energy with the QED-SCF methods. To confirm that, we have calculated individual energy contributions for the QED-HF and QED-CCSD methods. At the QED-HF level, fluctuations of the dipole self energy term, $\frac{1}{2}(\boldsymbol{\lambda} \cdot \Delta \boldsymbol{d})^2$, accounts for most of the overall changes due to cavity which is 0.45 kcal/mol and 0.86 kcal/mol for the methanol in the gas phase and in the explicit solvent, respectively. As seen from Table III, the total change due to cavity for the QED-HF method is 0.52 kcal/mol and 0.95 kcal/mol for methanol in the gas phase and in explicit solvent, respectively. Unlike the QED-HF, the energy contribution for the dipole self energy term calculated with the QED-CCSD method shows less deviation, 1.01 kcal/mol vs. 1.28 kcal/mol, for the methanol in the gas phase and the in explicit solvent, respectively. The dipolar coupling term (the fourth term in Eq. (1)) calculated with the QED-CCSD method has the smallest effect on the PBEn (~ 0.05 kcal/mol). For more information about the individual energy contributions to the PBEn we refer to Table S3. Lastly, the embedding methods where only MeOH is treated with the QED-CCSD method, are in excellent agreement with the QED-CCSD method for the full system.

IV. CONCLUSIONS

In this work, we have developed and implemented the QED-CCSD-in-SCF embedding method for polaritonic chemistry in which only the chemically important region is treated with the accurate but computationally expensive QED-CCSD method, whereas the environment is treated at the computationally more efficient QED-SCF level of the theory. We illustrate the performance of the method by studying the effect of cavity on the methyl and proton transfer reactions, as well as protonation reaction in an explicit solvent. The results obtained with the embedding method are in excellent agreement with results obtained using a more expensive QED-CCSD method. Moreover, we observe ten-fold computational speed-up of the QED-CCSD-in-SCF vs. QED-CCSD method for explored systems. Out of different studied QED-CCSD-in-SCF methods, the QED-CCSD-in-HF shows the best performance. We show that the correlation effects between the quantum particles is crucial for an accurate description of the effect of the optical cavity. We further show that the electron-photon correlation effect is relatively local in nature and only a small chemically important region has to be treated with the correlated QED-CCSD method for achieving a reliable accu-

racy. The development and analysis presented in this work will serve as a guideline for development of novel polaritonic quantum chemistry methods and it provides a valuable insights into polaritonic systems inside complex environments.

SUPPLEMENTARY MATERIAL

See the supplementary material for the reaction energies and barriers of the Menshutkin reaction and proton transfer reaction, energy contributions breakdown, and optimized structures.

ACKNOWLEDGMENTS

We acknowledge financial support from the Cluster of Excellence 'CUI: Advanced Imaging of Matter' of the Deutsche Forschungsgemeinschaft (DFG) - EXC 2056 - project ID 390715994. We also acknowledge support from the Max Planck–New York Center for Non-Equilibrium Quantum Phenomena. The Flatiron Institute is a division of the Simons Foundation.

AUTHOR DECLARATIONS

Conflict of Interest

The authors have no conflicts of interest to disclose.

DATA AVAILABILITY STATEMENT

The data that support the findings of this study are available within this article and its supplementary material.

[1]J. Lather, P. Bhatt, A. Thomas, T. W. Ebbesen, and J. George, "Cavity catalysis by cooperative vibrational strong coupling of reactant and solvent molecules," Angew. Chem. **58**, 10635–10638 (2019).
[2]J. A. Campos-Gonzalez-Angulo, R. F. Ribeiro, and J. Yuen-Zhou, "Resonant catalysis of thermally activated chemical reactions with vibrational polaritons," Nat. Commun. **10**, 1–8 (2019).
[3]C. Climent, J. Galego, F. J. Garcia-Vidal, and J. Feist, "Plasmonic nanocavities enable self-induced electrostatic catalysis," Angew. Chem. Int. Ed. **58**, 8698–8702 (2019).
[4]A. Thomas, J. George, A. Shalabney, M. Dryzhakov, S. J. Varma, J. Moran, T. Chervy, X. Zhong, E. Devaux, C. Genet, *et al.*, "Ground-state chemical reactivity under vibrational coupling to the vacuum electromagnetic field," Angew. Chem. **128**, 11634–11638 (2016).
[5]J. A. Hutchison, T. Schwartz, C. Genet, E. Devaux, and T. W. Ebbesen, "Modifying chemical landscapes by coupling to vacuum fields," Angew. Chem. **51**, 1592–1596 (2012).
[6]J. Fregoni, G. Granucci, E. Coccia, M. Persico, and S. Corni, "Manipulating azobenzene photoisomerization through strong light–molecule coupling," Nat. Chem. **9**, 1–9 (2018).
[7]A. Thomas, L. Lethuillier-Karl, K. Nagarajan, R. M. Vergauwe, J. George, T. Chervy, A. Shalabney, E. Devaux, C. Genet, J. Moran, *et al.*, "Tilting a ground-state reactivity landscape by vibrational strong coupling," Science **363**, 615–619 (2019).
[8]M. Ruggenthaler, N. Tancogne-Dejean, J. Flick, H. Appel, and A. Rubio, "From a quantum-electrodynamical light-matter description to novel spectroscopies," Nat. Rev. Chem. **2**, 1–16 (2018).
[9]L. Lacombe, N. M. Hoffmann, and N. T. Maitra, "Exact potential energy surface for molecules in cavities," Phys. Rev. Lett. **123**, 083201 (2019).
[10]T. E. Li, A. Nitzan, and J. E. Subotnik, "Collective vibrational strong coupling effects on molecular vibrational relaxation and energy transfer: Numerical insights via cavity molecular dynamics simulations," Angew. Chem. Int. Ed. **60**, 15533–15540 (2021).
[11]C. Schäfer, J. Flick, E. Ronca, P. Narang, and A. Rubio, "Shining light on the microscopic resonant mechanism responsible for cavity-mediated chemical reactivity," arXiv preprint arXiv:2104.12429 (2021).
[12]D. Sidler, M. Ruggenthaler, H. Appel, and A. Rubio, "Chemistry in quantum cavities: Exact results, the impact of thermal velocities, and modified dissociation," J. Phys. Chem. Lett. **11**, 7525–7530 (2020).
[13]D. Sidler, M. Ruggenthaler, C. Schäfer, E. Ronca, and A. Rubio, "A perspective on ab initio modeling of polaritonic chemistry: The role of non-equilibrium effects and quantum collectivity," arXiv preprint arXiv:2108.12244 (2021).
[14]J. D. Mallory and A. E. DePrince III, "Reduced-density-matrix-based ab initio cavity quantum electrodynamics," arXiv preprint arXiv:2204.00725 (2022).
[15]M. Ruggenthaler, J. Flick, C. Pellegrini, H. Appel, I. V. Tokatly, and A. Rubio, "Quantum-electrodynamical density-functional theory: Bridging quantum optics and electronic-structure theory," Phys. Rev. A **90**, 012508 (2014).
[16]J. Flick, M. Ruggenthaler, H. Appel, and A. Rubio, "Kohn–sham approach to quantum electrodynamical density-functional theory: Exact time-dependent effective potentials in real space," Proc. Natl. Acad. Sci. U.S.A. **112**, 15285–15290 (2015).
[17]J. Flick, M. Ruggenthaler, H. Appel, and A. Rubio, "Atoms and molecules in cavities, from weak to strong coupling in quantum-electrodynamics (qed) chemistry," Proc. Natl. Acad. Sci. U.S.A. **114**, 3026–3034 (2017).
[18]C. Schäfer, M. Ruggenthaler, V. Rokaj, and A. Rubio, "Relevance of the quadratic diamagnetic and self-polarization terms in cavity quantum electrodynamics," ACS Photonics **7**, 975–990 (2020).
[19]J. Flick, C. Schäfer, M. Ruggenthaler, H. Appel, and A. Rubio, "Ab initio optimized effective potentials for real molecules in optical cavities: Photon contributions to the molecular ground state," ACS Photonics **5**, 992–1005 (2018).
[20]A. J. Cohen, P. Mori-Sánchez, and W. Yang, "Insights into current limitations of density functional theory," Science **321**, 792–794 (2008).
[21]J. Hermann, R. A. DiStasio, and A. Tkatchenko, "First-principles models for van der waals interactions in molecules and materials: Concepts, theory, and applications," Chem. Rev. **117**, 4714–4758 (2017).
[22]C. Pellegrini, J. Flick, I. V. Tokatly, H. Appel, and A. Rubio, "Optimized effective potential for quantum electrodynamical time-dependent density functional theory," Phys. Rev. Lett. **115**, 093001 (2015).
[23]C. Schäfer, F. Buchholz, M. Penz, M. Ruggenthaler, and A. Rubio, "Making ab initio qed functional (s): Non-perturbative and photon-free effective frameworks for strong light-matter coupling," Proc. Natl. Acad. Sci. U.S.A. **118**, e2110464118 (2021).
[24]U. Mordovina, C. Bungey, H. Appel, P. J. Knowles, A. Rubio, and F. R. Manby, "Polaritonic coupled-cluster theory," Phys. Rev. Res. **2**, 023262 (2020).
[25]T. S. Haugland, E. Ronca, E. F. Kjønstad, A. Rubio, and H. Koch, "Coupled cluster theory for molecular polaritons: Changing ground and excited states," Phys. Rev. X **10**, 041043 (2020).
[26]R. J. Bartlett and M. Musiał, "Coupled-cluster theory in quantum chemistry," Rev. Mod. Phys. **79**, 291 (2007).
[27]T. S. Haugland, C. Schäfer, E. Ronca, A. Rubio, and H. Koch, "Intermolecular interactions in optical cavities: An ab initio qed study," J. Chem. Phys. **154**, 094113 (2021).
[28]A. E. DePrince III, "Cavity-modulated ionization potentials and electron affinities from quantum electrodynamics coupled-cluster theory," J. Chem. Phys. **154**, 094112 (2021).
[29]F. Pavošević and J. Flick, "Polaritonic unitary coupled cluster for quantum computations," J. Phys. Chem. Lett. **12**, 9100–9107 (2021).
[30]M. D. Liebenthal, N. Vu, and A. E. DePrince, "Equation-of-motion cavity quantum electrodynamics coupled-cluster theory for electron attachment," J. Chem. Phys. **156**, 054105 (2022).
[31]F. Pavošević, S. Hammes-Schiffer, A. Rubio, and J. Flick, "Cavity-modulated proton transfer reactions," J. Am. Chem. Soc. **144**, 4995–5002

(2022).
[32]L. O. Jones, M. A. Mosquera, G. C. Schatz, and M. A. Ratner, "Embedding methods for quantum chemistry: Applications from materials to life sciences," J. Am. Chem. Soc. **142**, 3281–3295 (2020).
[33]Q. Sun and G. K.-L. Chan, "Quantum embedding theories," Acc. Chem. Res. **49**, 2705–2712 (2016).
[34]T. E. Reinhard, U. Mordovina, C. Hubig, J. S. Kretchmer, U. Schollwöck, H. Appel, M. A. Sentef, and A. Rubio, "Density-matrix embedding theory study of the one-dimensional hubbard–holstein model," J. Chem. Theory Comput. **15**, 2221–2232 (2019).
[35]F. R. Manby, M. Stella, J. D. Goodpaster, and T. F. Miller III, "A simple, exact density-functional-theory embedding scheme," J. Chem. Theory Comput. **8**, 2564–2568 (2012).
[36]S. J. Lee, M. Welborn, F. R. Manby, and T. F. Miller III, "Projection-based wavefunction-in-dft embedding," Acc. Chem. Res. **52**, 1359–1368 (2019).
[37]S. J. Bennie, M. Stella, T. F. Miller III, and F. R. Manby, "Accelerating wavefunction in density-functional-theory embedding by truncating the active basis set," J. Chem. Phys. **143**, 024105 (2015).
[38]M. Bensberg and J. Neugebauer, "Automatic basis-set adaptation in projection-based embedding," J. Chem. Phys. **150**, 184104 (2019).
[39]D. Claudino and N. J. Mayhall, "Simple and efficient truncation of virtual spaces in embedded wave functions via concentric localization," J. Chem. Theory Comput. **15**, 6085–6096 (2019).
[40]H.-J. Werner, P. J. Knowles, F. R. Manby, J. A. Black, K. Doll, A. Heßelmann, D. Kats, A. Köhn, T. Korona, D. A. Kreplin, *et al.*, "The molpro quantum chemistry package," J. Chem. Phys. **152**, 144107 (2020).
[41]D. Craig and T. Thirunamachandran, *Molecular Quantum Electrodynamics: An Introduction to Radiation-molecule Interactions* (Dover Publications, 1998).
[42]F. Pavošević, T. Culpitt, and S. Hammes-Schiffer, "Multicomponent coupled cluster singles and doubles theory within the nuclear-electronic orbital framework," J. Chem. Theory Comput. **15**, 338–347 (2019).
[43]F. Pavošević, T. Culpitt, and S. Hammes-Schiffer, "Multicomponent quantum chemistry: Integrating electronic and nuclear quantum effects via the nuclear-electronic orbital method," Chem. Rev. **120**, 4222–4253 (2020).
[44]F. Pavošević and S. Hammes-Schiffer, "Multicomponent unitary coupled cluster and equation-of-motion for quantum computation." J. Chem. Theory Comput. **17**, 3252–3258 (2021).
[45]J. Galego, C. Climent, F. J. Garcia-Vidal, and J. Feist, "Cavity casimir-polder forces and their effects in ground-state chemical reactivity," Phys. Rev. X **9**, 021057 (2019).
[46]F. Benz, M. K. Schmidt, A. Dreismann, R. Chikkaraddy, Y. Zhang, A. Demetriadou, C. Carnegie, H. Ohadi, B. de Nijs, R. Esteban, J. Aizpurua, and J. J. Baumberg, "Single-molecule optomechanics in picocavities," Science **354**, 726–729 (2016).
[47]M. Richard-Lacroix and V. Deckert, "Direct molecular-level near-field plasmon and temperature assessment in a single plasmonic hotspot," Light: Science & Applications **9** (2020).
[48]S. Liu, A. Hammud, M. Wolf, and T. Kumagai, "Atomic point contact raman spectroscopy of a si(111)-7 7 surface," Nano Lett. **21**, 4057–4061 (2021).
[49]J. Griffiths, B. de Nijs, R. Chikkaraddy, and J. J. Baumberg, "Locating single-atom optical picocavities using wavelength-multiplexed raman scattering," ACS Photonics **8**, 2868–2875 (2021).
[50]V. Rokaj, D. M. Welakuh, M. Ruggenthaler, and A. Rubio, "Light–matter interaction in the long-wavelength limit: No ground-state without dipole self-energy," J. Phys. B **51**, 034005 (2018).
[51]M. A. D. Taylor, A. Mandal, W. Zhou, and P. Huo, "Resolution of gauge ambiguities in molecular cavity quantum electrodynamics," Phys. Rev. Lett. **125**, 123602 (2020).
[52]J. Fregoni, F. J. Garcia-Vidal, and J. Feist, "Theoretical challenges in polaritonic chemistry," ACS Photonics **9**, 1096–1107 (2022).
[53]M. Babiker, R. Loudon, and G. W. Series, "Derivation of the power-zienau-woolley hamiltonian in quantum electrodynamics by gauge transformation," Proceedings of the Royal Society of London. A. Mathematical and Physical Sciences **385**, 439–460 (1983).
[54]D. De Bernardis, T. Jaako, and P. Rabl, "Cavity quantum electrodynamics in the nonperturbative regime," Phys. Rev. A **97**, 043820 (2018).
[55]G. Andolina, F. Pellegrino, V. Giovannetti, A. MacDonald, and M. Polini, "Theory of photon condensation in a spatially varying electromagnetic field," Phys. Rev. B **102**, 125137 (2020).
[56]J. Feist, A. I. Fernández-Domínguez, and F. J. García-Vidal, "Macroscopic qed for quantum nanophotonics: emitter-centered modes as a minimal basis for multiemitter problems," Nanophotonics **10**, 477–489 (2021).
[57]T. Neuman, R. Esteban, D. Casanova, F. J. García-Vidal, and J. Aizpurua, "Coupling of molecular emitters and plasmonic cavities beyond the point-dipole approximation," Nano Letters **18**, 2358–2364 (2018).
[58]D. Claudino and N. J. Mayhall, "Automatic partition of orbital spaces based on singular value decomposition in the context of embedding theories," J. Chem. Theory Comput. **15**, 1053–1064 (2019).
[59]J. Pipek and P. G. Mezey, "A fast intrinsic localization procedure applicable for ab initio and semiempirical linear combination of atomic orbital wave functions," J. Chem. Phys. **90**, 4916–4926 (1989).
[60]R. S. Mulliken, "Electronic population analysis on lcao–mo molecular wave functions. i," J. Chem. Phys. **23**, 1833–1840 (1955).
[61]J. M. Waldrop, T. L. Windus, and N. Govind, "Projector-based quantum embedding for molecular systems: An investigation of three partitioning approaches," J. Phys. Chem. A **125**, 6384–6393 (2021).
[62]D. G. Smith, L. A. Burns, D. A. Sirianni, D. R. Nascimento, A. Kumar, A. M. James, J. B. Schriber, T. Zhang, B. Zhang, A. S. Abbott, *et al.*, "Psi4numpy: An interactive quantum chemistry programming environment for reference implementations and rapid development," J. Chem. Theory Comput. **14**, 3504–3511 (2018).
[63]R. Ditchfield, W. J. Hehre, and J. A. Pople, "Self-consistent molecular-orbital methods. ix. an extended gaussian-type basis for molecular-orbital studies of organic molecules," J. Chem. Phys. **54**, 724–728 (1971).
[64]P. C. Hariharan and J. A. Pople, "The influence of polarization functions on molecular orbital hydrogenation energies," Theor. Chim. Acta **28**, 213–222 (1973).
[65]V. A. Rassolov, M. A. Ratner, J. A. Pople, P. C. Redfern, and L. A. Curtiss, "6-31g* basis set for third-row atoms," J. Comput. Chem. **22**, 976–984 (2001).
[66]F. Neese, F. Wennmohs, U. Becker, and C. Riplinger, "The orca quantum chemistry program package," J. Chem. Phys. **152**, 224108 (2020).
[67]T. H. Dunning Jr, "Gaussian basis sets for use in correlated molecular calculations. i. the atoms boron through neon and hydrogen," J. Chem. Phys. **90**, 1007–1023 (1989).
[68]V. Parravicini and T.-C. Jagau, "Embedded equation-of-motion coupled-cluster theory for electronic excitation, ionisation, electron attachment, and electronic resonances," Mol. Phys. **119**, e1943029 (2021).
[69]J. P. Perdew, K. Burke, and M. Ernzerhof, "Generalized gradient approximation made simple," Phys. Rev. Lett. **77**, 3865 (1996).
[70]C. Adamo and V. Barone, "Toward reliable density functional methods without adjustable parameters: The pbe0 model," J. Chem. Phys. **110**, 6158–6170 (1999).
[71]C. Lee, W. Yang, and R. G. Parr, "Development of the colle-salvetti correlation-energy formula into a functional of the electron density," Phys. Rev. B **37**, 785–789 (1988).
[72]A. D. Becke, "Density-functional exchange-energy approximation with correct asymptotic behavior," Phys. Rev. A **38**, 3098–3100 (1988).
[73]E. Eizner, L. A. Martínez-Martínez, J. Yuen-Zhou, and S. Kéna-Cohen, "Inverting singlet and triplet excited states using strong light-matter coupling," Sci. Adv. **5**, eaax4482 (2019).
[74]T. Wu, W. Yan, and P. Lalanne, "Bright plasmons with cubic nanometer mode volumes through mode hybridization," ACS Photonics **8**, 307–314 (2021).
[75]M.-C. Kim, E. Sim, and K. Burke, "Ions in solution: Density corrected density functional theory (dc-dft)," J. Chem. Phys. **140**, 18A528 (2014).
[76]M.-C. Kim, H. Park, S. Son, E. Sim, and K. Burke, "Improved dft potential energy surfaces via improved densities," J. Phys. Chem. Lett. **6**, 3802–3807 (2015).
[77]R. C. Pennifold, S. J. Bennie, T. F. Miller III, and F. R. Manby, "Correcting density-driven errors in projection-based embedding," J. Chem. Phys. **146**, 084113 (2017).

QED-SCF calculation on the whole system A + B

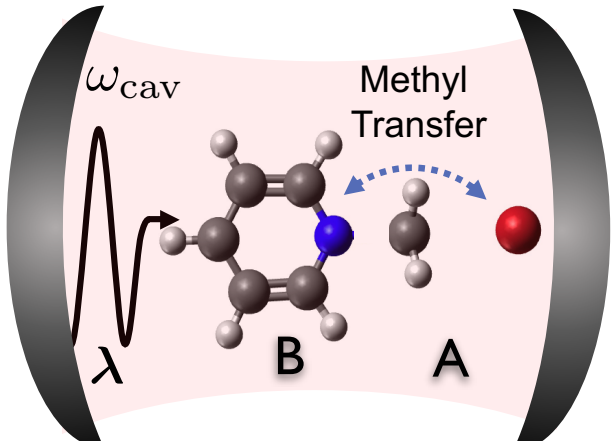

SPADE partitioning and assignment of occupied orbitals

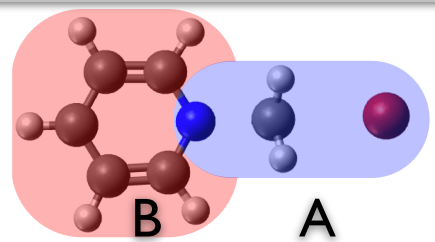

QED-SCF-in-QED-SCF energy calculation using Eq. (7)

Truncation of the virtual orbital space with CL procedure

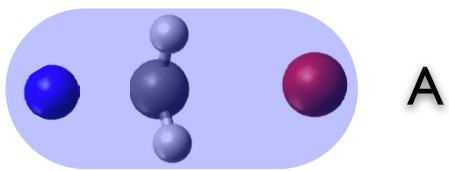

Perform QED-CCSD energy calculation on subsystem A using Eq. (9)

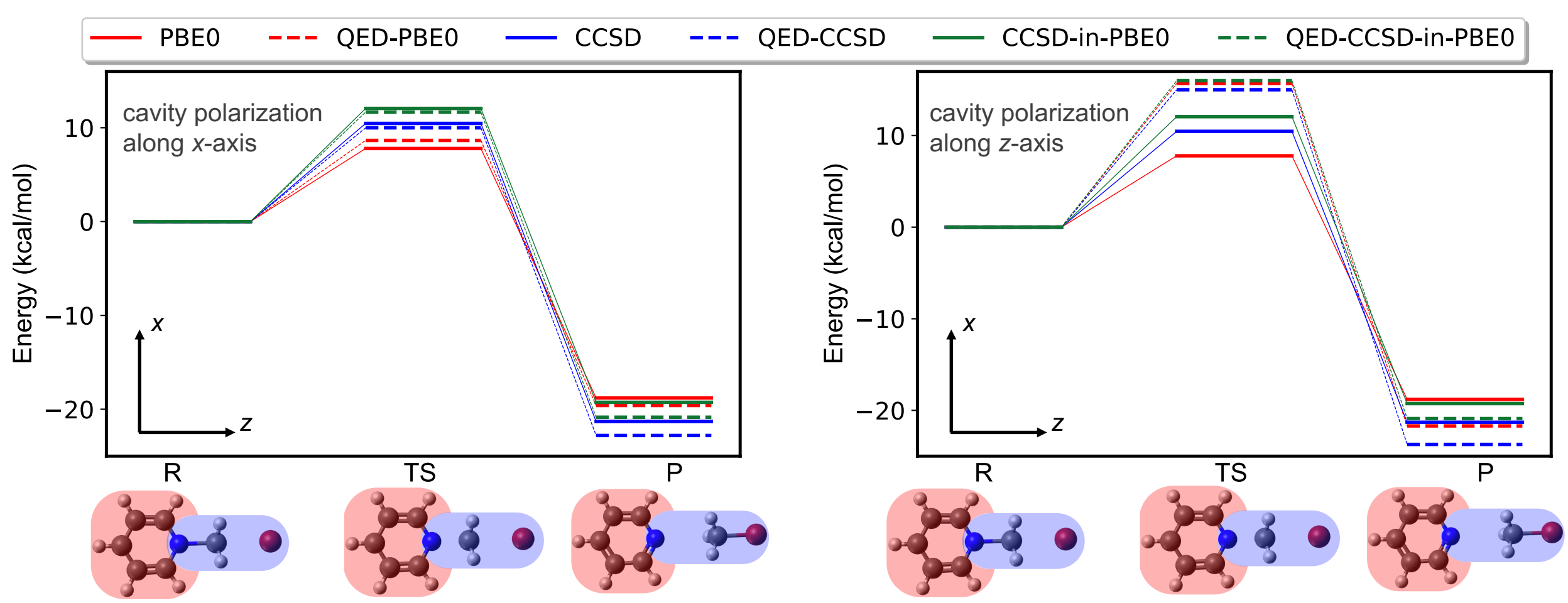
PBE0
QED-PBE0
CCSD
QED-CCSD
CCSD-in-PBE0
QED-CCSD-in-PBE0
cavity polarization
along x-axis
Energy (kcal/mol)
10
0
−10
−20
x
z
R
TS
P
cavity polarization
along z-axis
Energy (kcal/mol)
10
0
−10
−20
x
z
R
TS
P

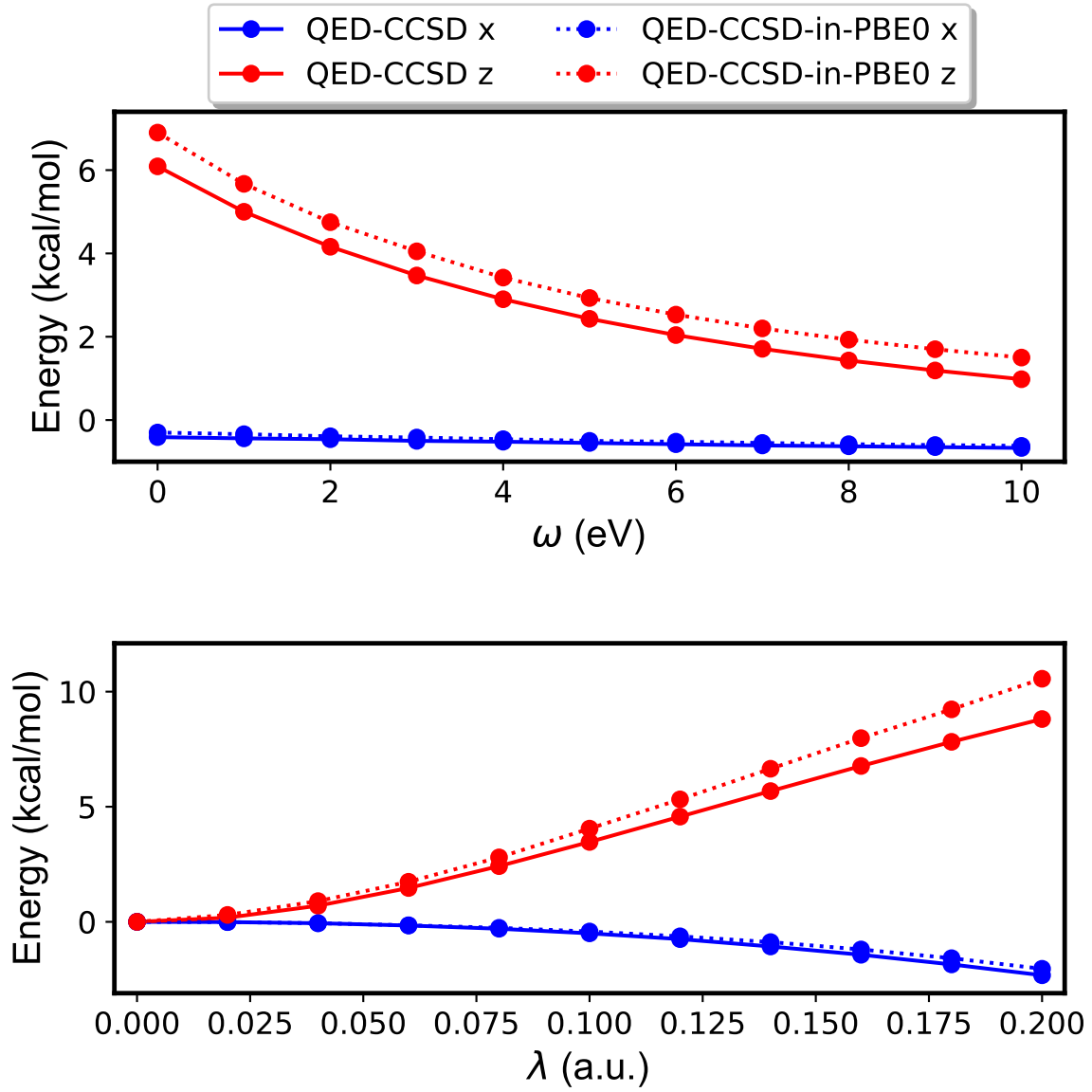
QED-CCSD x
QED-CCSD z
QED-CCSD-in-PBE0 x
QED-CCSD-in-PBE0 z
Energy (kcal/mol)
0
2
4
6
0
2
4
6
8
10
ω (eV)
Energy (kcal/mol)
0
5
10
0.000
0.025
0.050
0.075
0.100
0.125
0.150
0.175
0.200
λ (a.u.)

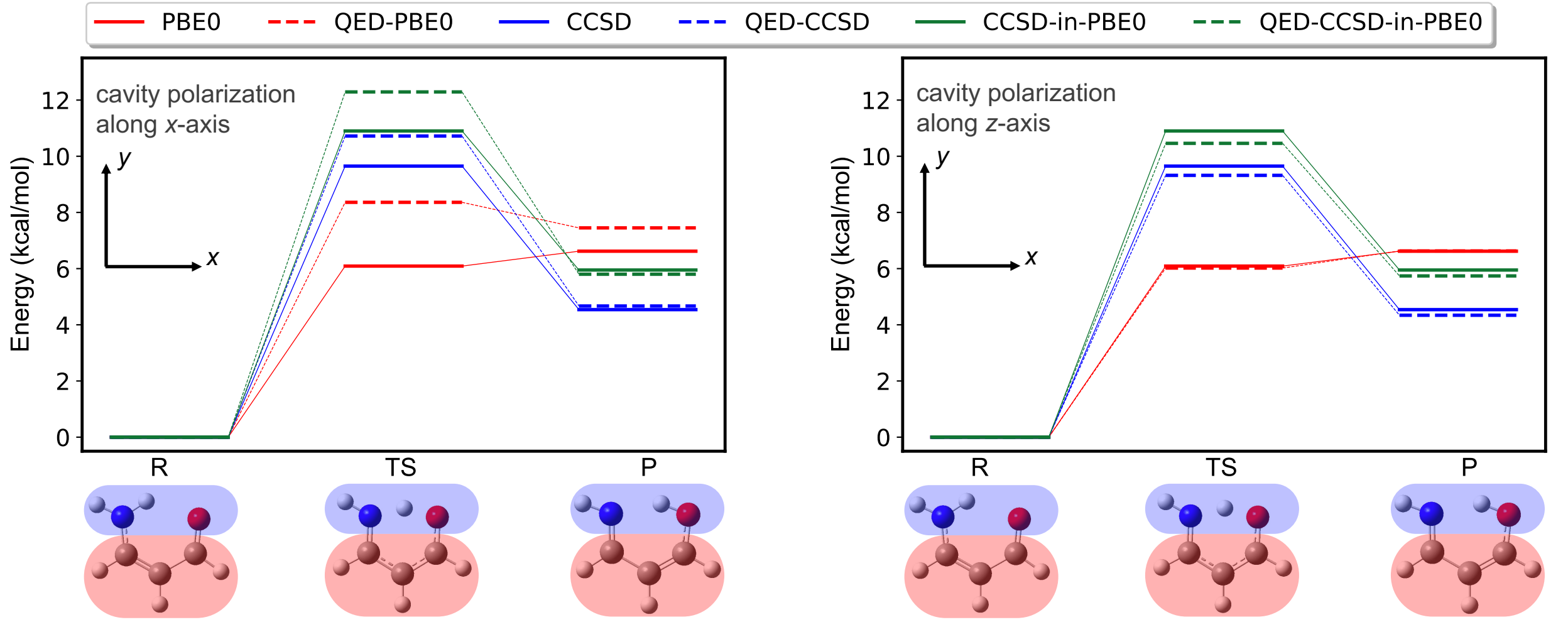
PBE0
QED-PBE0
CCSD
QED-CCSD
CCSD-in-PBE0
QED-CCSD-in-PBE0
cavity polarization
along x-axis
y
x
Energy (kcal/mol)
0
2
4
6
8
10
12
R
TS
P
cavity polarization
along z-axis
y
x
Energy (kcal/mol)
0
2
4
6
8
10
12
R
TS
P

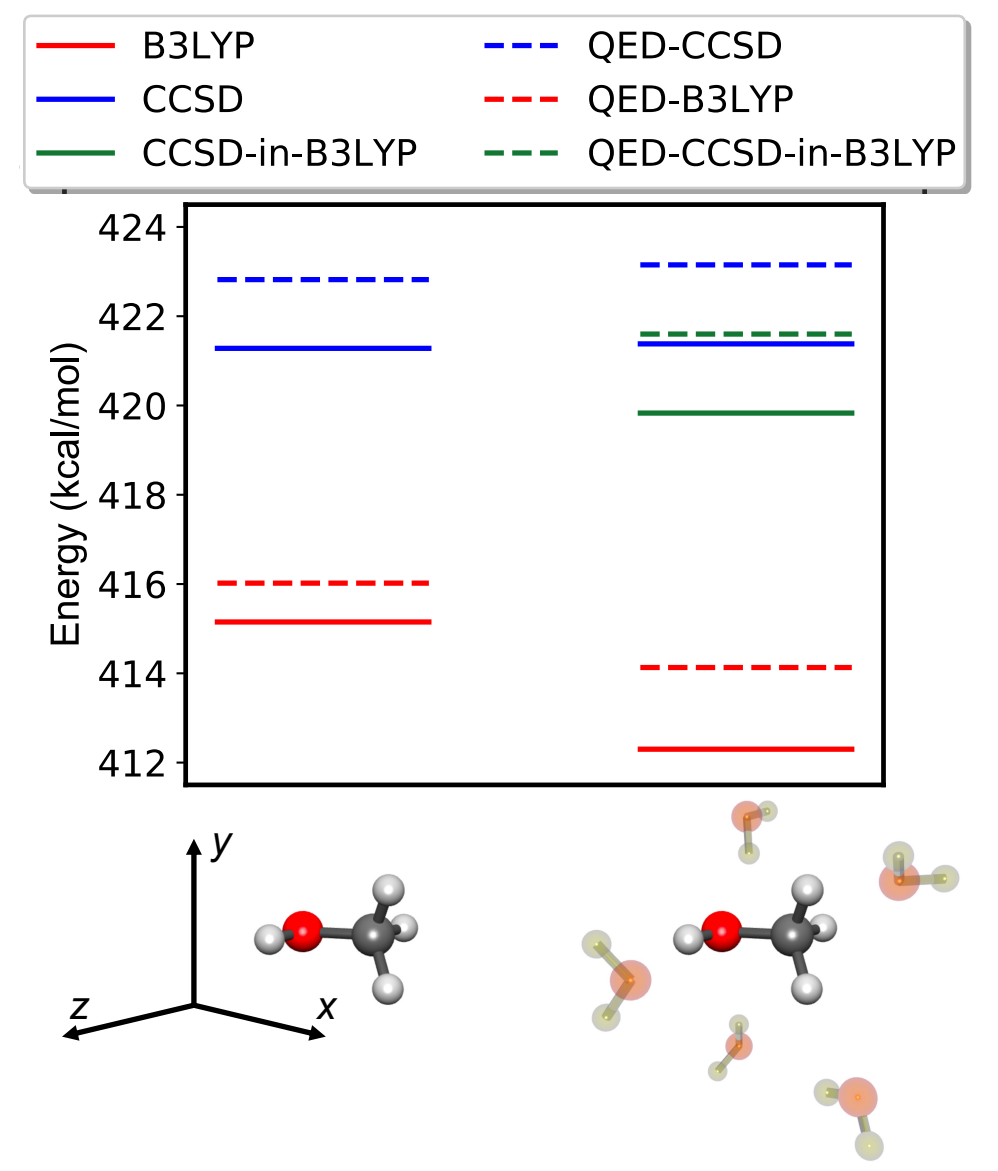
B3LYP
CCSD
CCSD-in-B3LYP
QED-CCSD
QED-B3LYP
QED-CCSD-in-B3LYP
Energy (kcal/mol)
424
422
420
418
416
414
412
y
z
x